

Enhancement of hydrogenation kinetics and thermodynamic properties of $\text{ZrCo}_{1-x}\text{Cr}_x$ ($x = 0-0.1$) alloys for hydrogen storage*

Linling Luo(罗林龄)¹, Xiaoqiu Ye(叶小球)¹, Guanghui Zhang(张光辉)², Huaqin Kou(寇化秦)², Renjin Xiong(熊仁金)², Ge Sang(桑革)^{2,†}, Ronghai Yu(于荣海)³, and Dongliang Zhao(赵栋梁)⁴

¹Science and Technology on Surface Physics and Chemistry Laboratory, Mianyang 621907, China

²Institute of Materials, China Academy of Engineering Physics, Mianyang 621900, China

³School of Materials Science and Engineering, Beihang University, Beijing 100191, China

⁴Department of Functional Material Research, Central Iron and Steel Research Institute, Beijing 100081, China

(Received 8 February 2020; revised manuscript received 25 April 2020; accepted manuscript online 13 May 2020)

The vacuum arc melting method was used to prepare $\text{ZrCo}_{1-x}\text{Cr}_x$ ($x = 0, 0.025, 0.05, 0.075, 0.1$) alloys. Afterward, the crystal structure, hydrogenation kinetics, thermodynamic properties, and disproportionation performance of $\text{ZrCo}_{1-x}\text{Cr}_x$ ($x = 0-0.1$) alloys were investigated. The x-ray diffraction spectra demonstrated that $\text{ZrCo}_{1-x}\text{Cr}_x$ ($x = 0-0.1$) alloys contained ZrCo and ZrCo_2 phases, and their corresponding hydrides consisted of ZrCoH_3 and ZrH phases. The activation behaviors of Cr-substituted samples were significantly promoted. The activation time of ZrCo was 7715 s while that of $\text{ZrCo}_{0.9}\text{Cr}_{0.1}$ was 195 s. The improvement of kinetics can be attributed to the catalytic hydrogenation of ZrCr_2 . The activation energy for the hydrogenation of ZrCo was $44.88\text{-kJ}\cdot\text{mol}^{-1}$ H_2 and decreased to $40.34\text{-kJ}\cdot\text{mol}^{-1}$ H_2 for $\text{ZrCo}_{0.95}\text{Cr}_{0.05}$. The plateau pressure and width of the pressure–composition–temperature curves decreased slightly as Cr content increased. The extent of disproportionation of ZrCo was 83.68% after being insulated at 798 K for 10 h and decreased slightly to 70.52% for $\text{ZrCo}_{0.9}\text{Cr}_{0.1}$. The improvement of anti-disproportionation performance can be attributed to increase in the activation energy of disproportionation from $167.46\text{-kJ}\cdot\text{mol}^{-1}$ H_2 for ZrCo to $168.28\text{-kJ}\cdot\text{mol}^{-1}$ H_2 for $\text{ZrCo}_{0.95}\text{Cr}_{0.05}$.

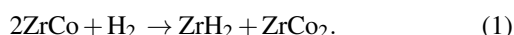
Keywords: hydrogen storage, ZrCo, Cr substitution, anti-disproportionation performance, activation behaviors

PACS: 88.30.R-, 89.30.Jj, 81.05.Bx

DOI: 10.1088/1674-1056/ab9289

1. Introduction

An intermetallic compound of ZrCo is proposed as a promising alternative to uranium (U) for hydrogen isotope storage in fusion energy in International Thermonuclear Experimental Reactor (ITER)^[1,2] as it offers advantages such as non-radioactivation, low pyrophoricity, low equilibrium absorption pressure (10^{-3} Pa), hydrogen capacity as high as 1.96 wt.%, and appropriate temperature of ~ 643 K for hydrogen desorption to 1 bar (1 bar = 10^5 Pa).^[3-6] The ZrCo alloy absorbs H_2 and forms ZrCoH_3 at room temperature. ZrCoH_3 releases H_2 and decomposes back to ZrCo at high temperatures. However, the presence of high temperature and high hydrogen pressure, or repeated H_2 absorption–desorption cycles, induce disproportionation,^[7-9] which can be described as follows:



The hydrogen-induced disproportionation (HID) reaction results in the decrease in the hydrogen capacity of the ZrCo alloy, which is attributed to the high stabilities of ZrH_2 and

ZrCo_2 .^[8] It took 12 h for ZrH_2 and ZrCo_2 to completely change back to the ZrCo phase under continuous evacuation at 773 K,^[10] which leads to tritium permeation at high temperatures and the loss of rare tritium. The disproportionation reaction restricts the practical application of the ZrCo alloy. Therefore, it is necessary to improve the thermal stability to resist HID for ZrCo. As temperature and hydrogen pressure have a remarkable influence on the kinetics and extent of disproportionation,^[11] there are three ways to avoid or prevent HID. One is by increasing the hydrogen desorption pressure, using ZrCoH_3 at relatively low temperatures to avoid high temperature disproportionation. The other is improving the thermal stability of ZrCoH_3 , which can prevent HID at high temperatures. The last is decreasing the hydrogen pressure, when using ZrCoH_3 at high temperature.^[12] Some studies revealed that the addition of alloying elements could improve the hydrogen storage performance of alloys effectively.^[13,14] For instance, transition elements such as Ti, Hf, Ni, Mn, Sc, Fe, Mo, Cu, and Nb were used to replace Zr or Co, or both Zr and Co to improve the ability of anti-disproportionation.^[8,15-25] It was reported that the

*Project supported by the National Natural Science Foundation of China (Grant Nos. 21573200, 2017YFE0301505, 21601165, 21401173, 21573200, and 51731002).

†Corresponding author. E-mail: anglesg@163.com

substitution of Ti, Hf, and Nb for Zr improve the ability of anti-disproportionation effectively.^[8,15,19] Particularly, the Ti substitution showed the best anti-disproportionation property; only 5.54% Zr_{0.8}Ti_{0.2}Co alloy was disproportionated after the operated disproportionation reaction at 773 K under a hydrogen pressure of 60 kPa for 1000 min.^[26] The first-principle method was employed to study the mechanism of disproportionation.^[27,28] The calculated results showed that the substitutions of Ti for Zr increased ductility of the alloy,^[29] decreased the 8e tetrahedron volume and increased the length of Zr–H bond in 8e side, which are helpful to improve the cycling performance of ZrCo alloy.

Besides disproportionation, the ZrCo alloy exhibits stagnant hydrogen absorption kinetics compared with U.^[30] It took 7 h for the ZrCo ingot to finish the first hydrogenation process.^[9] The response time of U was about thrice shorter than that of the activated ZrCo alloy.^[1,31] Particularly, surface modification and mechanical ball milling are effective techniques to improve the kinetic properties of hydrogen storage materials.^[32,33] However, the ZrCo ingot should be powdered before surface modification and mechanical ball milling, and the ZrO₂ membrane formed and deteriorated the initial activation behaviors of the ZrCo alloy.^[34] Alloying, such as the substitution of Mn and Mo for Co, or Hf and Nb for Zr,^[18,19,23,35] can also significantly improve the hydrogenation kinetics of ZrCo ingot.

In studies conducted by Yao *et al.* and Lv,^[36,37] Cr was used to replace Co. Hydrogen absorption kinetics were greatly improved, while the anti-disproportionation performance deteriorated. Nevertheless, the effects of Cr content substitutes for Co on kinetics and HID, as well as the mechanism on improving kinetics and anti-disproportionation properties, remain unknown. This study examined the crystal structure, hydrogenation kinetics, and thermodynamic performance, as well as the ability of the anti-disproportionation of ZrCo_{1-x}Cr_x ($x = 0-0.1$) alloys. Cr-alloyed alloys show better kinetics and ability of anti-disproportionation than that of ZrCo. Moreover, the mechanism on improving kinetics and anti-disproportionation properties of ZrCo_{1-x}Cr_x ($x = 0-0.1$) alloys has also been proposed.

2. Experimental procedures

The vacuum arc melting method was used to prepare ZrCo_{1-x}Cr_x ($x = 0, 0.025, 0.05, 0.075, \text{ and } 0.1$) alloys. The stoichiometric amount of Zr, Cr, and Co ($\geq 99.9\%$) metals was placed into the arc furnace, and then the furnace was pumped at $< 10^{-3}$ Pa and flushed with argon ($\geq 99.99\%$) three times. Melted zirconium was used to consume the impurities before melting. To ensure the homogeneity of alloys, the ingots were re-melted five times. The weight of each ingot is ~ 15 g.

To measure the initial activation properties, the ingots were hydrogenated under hydrogen pressure of 4 bar at 348 K

after vacuuming for 1 h at 773 K. The hydrides were crushed to powder in glovebox under argon atmosphere mechanically, and H₂ was removed using vacuuming at 773 K for 1 h to obtain the powdered alloys.

X-ray diffraction (XRD, X'Pert-PRO) for the powdered alloys and hydrides were recorded using the Cu K_{α} radiation at 40 kV and 30 mA. The surface morphologies, Zr, Co, and Cr distributions were investigated by FEI Quanta250 scanning electron microscope (SEM) equipped with energy dispersive spectrum (EDS).

The typical experiment of hydrogen desorption pressure–composition–temperature (PCT) curves and HID was conducted on Sievert's-type apparatus. The hydrides of ZrCo_{1-x}Cr_x ($x = 0-0.1$) alloys were put into the vessel and dehydrogenated by vacuuming for 1 h at 773 K and then hydrogenated again under a hydrogen pressure of 5 bar at temperatures of 548 K, 573 K, and 598 K. Finally, the vessel was insulated at the target temperatures to obtain PCT curves. To investigate the disproportionation behaviors of ZrCo_{1-x}Cr_x ($x = 0-0.1$)–H systems, the hydrides of alloys were put into the vessel. Then, the vessel was pumped at < 1 Pa. The hydrides of alloys were rapidly heated up to the target temperatures for the desorption processes and insulated for different time. During the insulation processes, ZrCoH₃ decomposed to ZrCo and H₂, prompting the disproportionation reaction (1), and the hydrogen pressure decreased gradually. The disproportionation reaction was considered to be completed when the hydrogen pressure of the system remained unchanged for about half an hour.

3. Results and discussion

3.1. Materials characterization

Figure 1 demonstrates the XRD spectra of the alloys with the composition of ZrCo_{1-x}Cr_x ($x = 0-0.1$) obtained from the hydrides dehydrogenated at 773 K for 1 h under dynamic vacuum; their corresponding hydrides are shown in Fig. 2. According to the Joint Committee on Powder Diffraction Standards (JCPDS) file Nos. 65-7272, 33-0416, and 65-0808, Cr-substituted alloys contain ZrCo phase with bcc (CsCl-type) structure and a fraction of ZrCo₂ secondary phase. A single ZrCo phase is difficult to prepare because ZrCo₂, which is more stable than ZrCo, is formed in the cobalt-rich side when it cools down from melting point to room temperature.^[17,38] Fortunately, the diffraction peaks of ZrCo₂ decrease gradually with the increasing content of Cr. The melted ZrCo_{1-x}Cr_x ($x = 0.025-0.1$) alloys cooled from more than 3000 K to room temperature, eutectic reaction started at 1605 K, and formed ZrCr₂.^[39] There is competition between the formation of ZrCr₂ and ZrCo₂, the formation of ZrCr₂ consumed the Zr atoms which formed ZrCo₂ in ZrCo alloy and restrained the formation of ZrCo₂ phase. The ZrCr₂ phase, which was

also observed in $\text{ZrCo}_{0.8}\text{Cr}_{0.2}$ alloy,^[36] stacked in the inter-phase boundaries and acted as pathways for hydrogen transportation in $\text{ZrCo}_{1-x}\text{Cr}_x$ ($x = 0.025-0.1$) alloys.^[37] The ZrCr_2 phase may be too small in quantity to be observed by XRD in $\text{ZrCo}_{1-x}\text{Cr}_x$ ($x = 0.025-0.1$) alloys. In addition, the diffraction peaks of $\text{ZrCo}_{1-x}\text{Cr}_x$ ($x = 0-0.1$) alloys shift slightly toward the lower angle direction since the atomic radius of Cr (128 pm) is higher than that of Co (125 pm). Table 1 lists the calculated lattice parameters and cell volume of the ZrCo phase. The lattice parameters and cell volume increase slightly as the Cr content increases. As shown in Fig. 2, with the exception of the $\text{ZrCo}_{0.9}\text{Cr}_{0.1}-\text{H}$ system, the hydrides of alloys mainly comprise of ZrCoH_3 phase. Moreover, ZrH phase is detected in the $\text{ZrCo}_{0.9}\text{Cr}_{0.1}-\text{H}$ system, and the same ZrH phase was observed in the $\text{ZrCo}_{1-x}\text{Mo}_x-\text{H}$ system.^[23] The intensities of the ZrCo_2 phase gradually decrease with the increase in the Cr concentration, which agrees with our previous analysis.

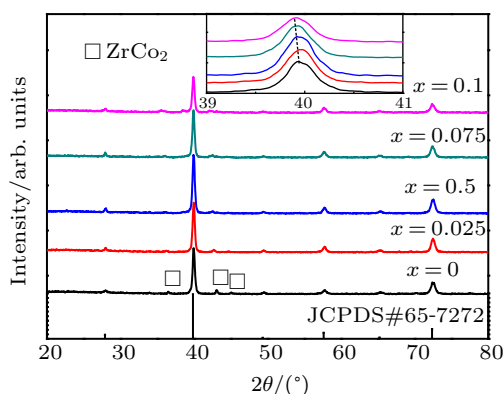


Fig. 1. XRD spectra of $\text{ZrCo}_{1-x}\text{Cr}_x$ ($x = 0-0.1$) alloys.

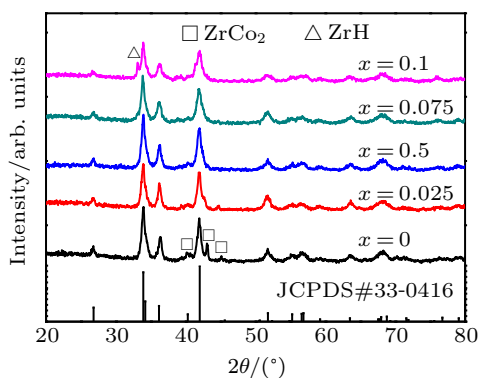


Fig. 2. XRD spectra of $\text{ZrCo}_{1-x}\text{Cr}_x$ ($x = 0-0.1$)-H systems.

Table 1. Lattice parameters and cell volume of ZrCo phase in $\text{ZrCo}_{1-x}\text{Cr}_x$ ($x = 0-0.1$) alloys.

| Samples | Lattice parameters/Å | Cell volume/Å ³ |
|-------------|----------------------|----------------------------|
| $x = 0$ | 3.1912 | 32.4984 |
| $x = 0.025$ | 3.1917 | 32.5137 |
| $x = 0.05$ | 3.1921 | 32.5259 |
| $x = 0.075$ | 3.1936 | 32.5718 |
| $x = 0.1$ | 3.1944 | 32.5963 |

The typical SEM image and corresponding EDS mappings carried out at the surface of the $\text{ZrCo}_{0.05}\text{Cr}_{0.05}$ ingot are displayed in Fig. 3. It is evident from Fig. 3 that Zr and Co distribute uniformly, which implies that ZrCo and ZrCo_2 phases distribute homogeneously. Table 2 lists the average chemical compositions of $\text{ZrCo}_{1-x}\text{Cr}_x$ ($x = 0-0.1$) samples obtained using EDS. The calculated results agree with the normal compositions. The EDS microanalysis shows the homogeneity of Zr and Co, whereas the elemental mapping of Cr suggests that segregation is present for Cr, which is in accordance with the existence of the ZrCr_2 phase.

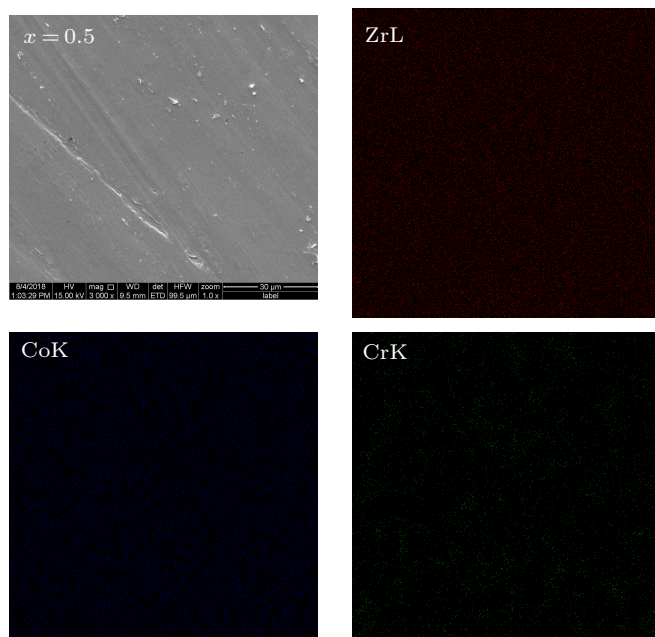


Fig. 3. EDS mappings of $\text{ZrCo}_{0.95}\text{Cr}_{0.05}$ alloy.

Table 2. Average chemical composition (atom%) for $\text{ZrCo}_{1-x}\text{Cr}_x$ ($x = 0-0.1$) alloys.

| Samples | Zr L | Co K | Cr K |
|-------------|-------|-------|------|
| $x = 0$ | 48.36 | 51.64 | |
| $x = 0.025$ | 48.08 | 50.14 | 1.78 |
| $x = 0.05$ | 47.50 | 49.34 | 3.16 |
| $x = 0.075$ | 47.40 | 48.12 | 4.48 |
| $x = 0.1$ | 48.24 | 46.26 | 5.50 |

3.2. Initial activation behaviors

$\text{ZrCo}_{1-x}\text{Cr}_x$ ($x = 0-0.1$) ingots were activated directly, without any mechanical treatments, by hydrogenation under a hydrogen pressure of 4 bar at 348 K after vacuuming for 1 h at 773 K.

As shown in Fig. 4, the concentration of Cr influences the initial activation behaviors and the hydrogen storage capacity significantly. It takes ~ 6 s for the $\text{ZrCo}_{0.9}\text{Cr}_{0.1}$ alloy to begin hydrogen absorption at 348 K under a hydrogen pressure of 4 bar, while the ZrCo alloy requires 30 s under the same conditions. Furthermore, the activation time decreases from 7715 s for the ZrCo ingot to 195 s for the $\text{ZrCo}_{0.9}\text{Cr}_{0.1}$ alloy, which is approximately 40 times less. In addition, it takes

3138 s, 1316 s, and 759 s for $\text{ZrCo}_{0.975}\text{Cr}_{0.025}$, $\text{ZrCo}_{0.95}\text{Cr}_{0.05}$, and $\text{ZrCo}_{0.925}\text{Cr}_{0.075}$ samples, respectively, to finish the activation. The initial activation behaviors are listed in Table 3. Hence, there is a great improvement on the activation behaviors of alloys in which Cr substitutes only a small fraction of Co. Thus, Cr-alloying provides a convenient method to activate the alloys without any mechanical treatments. This remarkable change in hydrogenation kinetics for Cr-alloyed ingots can be explained from two perspectives. The surface analysis of ZrCr_2 showed that Zr, which was oxidized easily and had lower surface energy, diffused to the surface and bound the oxygen.^[40] The oxidized Zr was separated at the surface of metallic-Cr precipitation.^[41] The hydrogen migrated through the decomposed surface and dissociated at the Cr or ZrCr_2 sub-surface, which has excellent catalytic activity with respect to the $\text{H}_2 \rightarrow 2\text{H}$ reaction.^[40] In addition, the existence of ZrCr_2 can not only catalyze the $\text{H}_2 \rightarrow 2\text{H}$ reaction but also act as pathways for hydrogen diffusion.^[42] Moreover, the increased friability of alloys may be considered for the improvement of hydrogenation kinetics, which decreases the size of hydrides and shortens the distance of hydrogen diffusion. However, the hydrogen capacity of $\text{ZrCo}_{1-x}\text{Cr}_x$ ($x = 0-0.1$) alloys decrease with the increasing content of Cr. The saturated hydrogen capacity at 348 K for the ZrCo alloy is 2.896 (H(f.u.)), and it decreases to 2.679 (H(f.u.)) for the $\text{ZrCo}_{0.9}\text{Cr}_{0.1}$ alloy. This reduction can be attributed to the existence of ZrCr_2 and the formation of the ZrH phase during hydrogenation. The hydrogen storage capabilities of $\text{ZrCo}_{1-x}\text{Cr}_x$ ($x = 0-0.1$) alloys under a hydrogen pressure of 4 bar at 348 K are listed in Table 3.

Table 3. Initial activation behaviors of $\text{ZrCo}_{1-x}\text{Cr}_x$ ($x = 0-0.1$) alloys under 4-bar H_2 at 348 K. Incubation period: the time needed to begin hydrogen absorption. Activation time: the time needed to reach 95% of saturated hydrogen capacity.

| Samples | Incubation period/s | Activation time/s | Hydrogen absorption capability/(H(f.u.)) |
|-------------|---------------------|-------------------|--|
| $x = 0$ | 30 | 7715 | 2.896 |
| $x = 0.025$ | 14 | 3138 | 2.822 |
| $x = 0.05$ | 9 | 1316 | 2.803 |
| $x = 0.075$ | 7 | 759 | 2.774 |
| $x = 0.1$ | 6 | 195 | 2.679 |

The hydrogenation reaction of the ZrCo alloy can be considered as a solid-gas reaction, which includes the transportation of hydrogen molecules on the alloy surface, dissociation of hydrogen molecules to atoms, and diffusion of hydrogen atoms through surface. The hydriding process is controlled by the $\text{H}_2 \rightarrow 2\text{H}$ reaction on the surface of Zr-based alloys.^[43,44] The better hydrogenation kinetics of Cr-alloyed alloys (Fig. 4) can be ascribed to the catalytic hydrogenation reaction of ZrCr_2 for the dissociation of hydrogen molecules to atoms. Owing to the acceleration of the controlling dissociation process, the kinetic properties of Cr-alloyed alloys are improved in the initial activation stage.

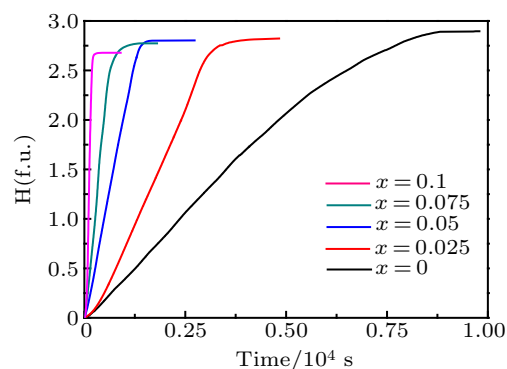


Fig. 4. First hydrogenation kinetics of $\text{ZrCo}_{1-x}\text{Cr}_x$ ($x = 0-0.1$) alloys under 4-bar H_2 at 348 K.

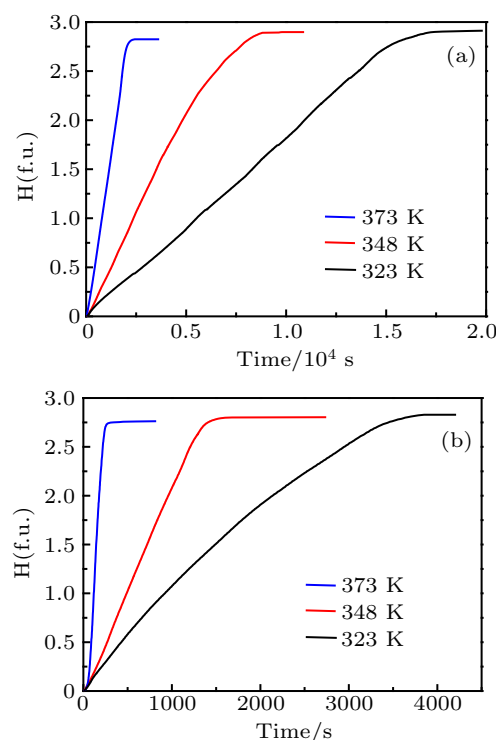


Fig. 5. Initial hydriding kinetic curves for ZrCo (a) and $\text{ZrCo}_{0.95}\text{Cr}_{0.05}$ (b) alloys at 323 K, 348 K, and 373 K.

To investigate the mechanism of hydrogenation kinetics further, systematic kinetics tests for ZrCo and $\text{ZrCo}_{0.95}\text{Cr}_{0.05}$ alloys were performed. The results are shown in Fig. 5. The hydrogenation kinetics of ZrCo and $\text{ZrCo}_{0.95}\text{Cr}_{0.05}$ alloys were measured at 323 K, 348 K, and 373 K. A proper kinetics model has been adopted to fit the kinetics curves. Moreover, the Johnson-Mehl-Avrami-Kolmogorov (JMAK) model and the Arrhenius theory^[32,45,46] are applied to calculate the activation energy for hydrogenation (E_{a1}). Based on the JMAK model, hydrogenation kinetics can be shown in an equation (Eq. (1)) as follows:

$$\ln[-\ln(1 - \alpha)] = \eta \ln k + \eta \ln t, \quad (2)$$

where α is the reaction factor, k is the rate constant, η is the reaction order, and t is the reaction time. According to Eq. (1), the fitted hydrogenation kinetics curves for ZrCo and

ZrCo_{0.95}Cr_{0.05} alloys at 323 K, 348 K, and 373 K are displayed in Fig. 6. As shown in Fig. 6, two samples at different temperatures denote straight lines with an intercept $\eta \ln k$ and a slope η , and $\ln k$ can be obtained. The E_{a1} for hydrogenation is calculated from the Arrhenius equation (Eq. (2)):

$$k = A \exp(-E_{a1}/RT), \quad (3)$$

where A is the temperature-independent coefficient, R is the gas constant, and T is the temperature. According to Eq. (2), the linear plots of $\ln k$ versus $1000/T$ for the hydrogenation of two samples at different temperatures are shown in Fig. 7.

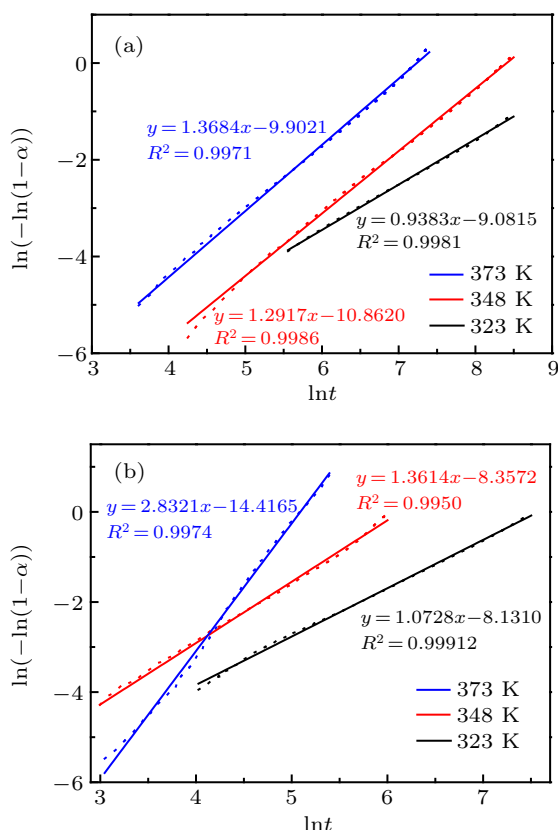


Fig. 6. Plots of $\ln(-\ln(1-\alpha))$ versus $\ln t$ for the hydrogenation of ZrCo (a) and ZrCo_{0.95}Cr_{0.05} (b) alloys.

As shown in Figs. 6 and 7, the fits (R^2) of straight lines and plots are larger than 0.995, implying that the experimental data evaluated from the JMAK model and the Arrhenius theory are reliable. The E_{a1} for hydrogenation of the ZrCo alloy, which was calculated from the slope ($-E_{a1}/R$) of fitted lines, is determined to be 44.88-kJ·mol⁻¹ H₂, while that of ZrCo_{0.95}Cr_{0.05} alloy decreases to 40.34-kJ·mol⁻¹ H₂. E_{a1} is regarded as the energy barrier for hydrogenation. Only when the ambient energy exceeds the energy barrier, the hydriding process can take place. The change in E_{a1} is used to estimate the driving force of hydrogenation. E_{a1} decreases after the Cr substitution, suggesting that the substitution of Cr for Co reduces the energy barrier for hydrogenation, which helps improve hydrogen absorption kinetics.

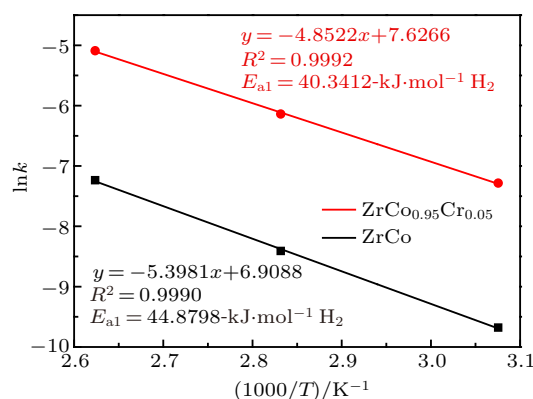


Fig. 7. Plots of $\ln k$ versus $1000/T$ for the hydrogenation of ZrCo and ZrCo_{0.95}Cr_{0.05} alloys.

3.3. Thermodynamic characteristics

The thermodynamic behaviors are key indicators for the ZrCo alloy. The hydrogen desorption PCT curves were measured to study the effects of the concentration of Cr on thermodynamic behaviors. Considering the rather low desorption pressure of the ZrCo alloy, the PCT curves were measured at 548 K, 573 K, and 598 K. As illustrated in Fig. 8, all the hydrides with different Cr content measurements show a single plateau within the temperature range, which is corresponding to the decomposition of the ZrCoH₃ phase, suggesting that the impure ZrCo₂ and ZrH phases have no effect on the desorption curves. The desorption process can be referred to as the decomposition of the ZrCoH₃ phase because the ZrCo₂ phase does not react with hydrogen under normal conditions, while ZrH decomposes at ~ 460 K.^[23] There is a direct correlation between the Cr content and the plateau width and plateau pressure in these alloys. The width and pressure of the desorption plateau, as well as hydrogen storage capacity, decrease with the increasing content of Cr, which is in accordance with Weng *et al.* and Luo *et al.*^[18,23] As shown in Fig. 8, the hydrogen storage capacity at 548 K under a hydrogen pressure of 5 bar decreases from 2.714 (H(f.u.)) for ZrCo to 2.559 (H(f.u.)) for ZrCo_{0.9}Cr_{0.1}. Meanwhile, the pressure and width of the plateau decrease slightly. Compared with the ZrCo alloy, the length of Zr-Co bonds was maintained in Zr_{0.8}CoSc_{0.2} alloy (from 2.74 Å to 2.72 Å),^[47] and the Zr_{0.8}Sc_{0.2}Co-H system almost maintained the thermodynamic characteristics. According to Table 1, the lattice parameters, the cell volume, and the length of the Zr-Co bond of ZrCo_{1-x}Cr_x ($x = 0.025-0.1$)-H systems are deduced to increase slightly, which makes the size of interstitial sites larger. The stability of the hydrides will be increased,^[48] and thus, the desorption plateau pressures of ZrCo_{1-x}Cr_x ($x = 0-0.1$)-H systems will decrease gradually. However, there has been no extant study about length of the Zr-Co bond in ZrCo_{1-x}Cr_x ($x = 0.025-0.1$) alloys that directly supports our explanation. In addition, with the increasing Cr content in the samples, the residual hydrogen in matrix at 548 K increases from 0.228 for ZrCo to 0.608 (H(f.u.)) for ZrCo_{0.9}Cr_{0.1}, which can be attributed to the different affinities with hydrogen between Co and Cr.

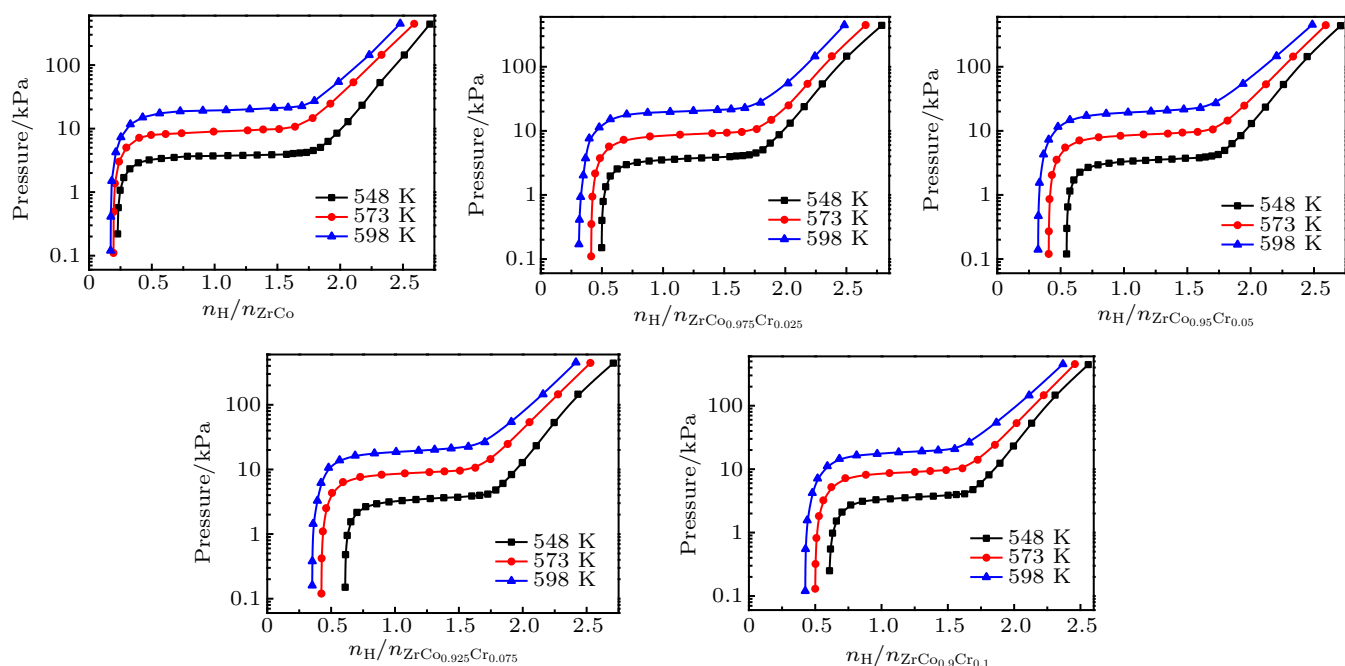


Fig. 8. PCT curves of $\text{ZrCo}_{1-x}\text{Cr}_x$ ($x=0-0.1$)-H systems.

To investigate the temperature dependence of the desorption plateau pressure for $\text{ZrCo}_{1-x}\text{Cr}_x$ ($x=0-0.1$)-H systems, ΔH and ΔS for the hydrogen desorption of the hydrides are obtained by the Van't Hoff equation (Eq. (3)), which can be expressed as

$$\ln(p/p^0) = -\Delta H/RT + \Delta S/R, \quad (4)$$

where p is the plateau pressure and ΔH and ΔS are the changes in enthalpy and entropy for the dehydriding reaction, respectively. Van't Hoff plots for the hydrogen desorption of $\text{ZrCo}_{1-x}\text{Cr}_x$ ($x=0-0.1$)-H systems are shown in Fig. 9.

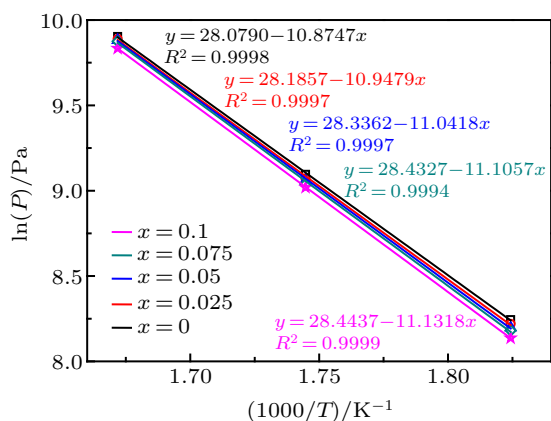


Fig. 9. Van't Hoff curves for $\text{ZrCo}_{1-x}\text{Cr}_x$ ($x=0-0.1$)-H systems.

The fitted curves demonstrate straight lines with an intercept ($-\Delta H/R$) and a slope ($\Delta S/R$), and the fits (R^2) of the straight lines and plots are > 0.999 . The calculated and reported ΔH and ΔS for hydride desorption are listed in Table 4. There is a direct connection between the thermodynamic data and the Cr content. ΔH and ΔS for the hydrogen desorption

of the ZrCo alloy are 90.41-kJ/mol H_2 and 233.45-kJ/mol-K H_2 , which are comparable to Yao *et al.*^[19] ΔH and ΔS gradually increase to 92.54-kJ/mol H_2 and 236.48-kJ/mol-K H_2 for the $\text{ZrCo}_{0.9}\text{Cr}_{0.1}$ -H system, which is in accordance with the reduction of plateau pressure. ΔH and ΔS are considered to be related to the stability of hydrides. ΔH and ΔS increase slightly with the increasing Cr content; *i.e.*, the Cr doping makes no significant difference in the thermodynamic characteristics.

Table 4. Thermodynamic characteristics for hydrogen desorption of $\text{ZrCo}_{1-x}\text{Cr}_x$ ($x=0-0.1$)-H systems.

| Systems | ΔH /(kJ/mol H_2) | ΔS /(kJ/mol-K H_2) |
|---|------------------------------------|--------------------------------------|
| ZrCo-H ^[19] | 89.71 | 226.16 |
| ZrCo-H | 90.41 | 233.45 |
| $\text{ZrCo}_{0.975}\text{Cr}_{0.025}$ -H | 91.02 | 234.34 |
| $\text{ZrCo}_{0.95}\text{Cr}_{0.05}$ -H | 91.80 | 235.59 |
| $\text{ZrCo}_{0.925}\text{Cr}_{0.075}$ -H | 92.33 | 236.38 |
| $\text{ZrCo}_{0.9}\text{Cr}_{0.1}$ -H | 92.54 | 236.48 |

3.4. Disproportionation behaviors

The practical application of the ZrCo alloy is limited by the poor anti-disproportionation properties. The disproportionation performance mainly depends on the operating temperature and hydrogen pressure.^[9] We chose 798 K and a hydrogen pressure of > 1 bar as experimental conditions. To compare the ability of the anti-disproportionation of $\text{ZrCo}_{1-x}\text{Cr}_x$ ($x=0-0.1$) alloys, all the hydrides were heated to 798 K, insulated for 10 h, and cooled to room temperature in the furnace.

Figure 10 demonstrates the evolution of hydrogen pressure. ZrCoH_3 decomposes to ZrCo and H_2 ; the hydrogen pressure increases dramatically with increasing temperature

and attains the maximum value, which is corresponding to the equilibrium pressure of $\text{ZrCo}_{1-x}\text{Cr}_x$ ($x = 0-0.1$)-H systems at 798 K. The disproportionation reaction experiences an incubation period; the residual hydrogen atoms in matrix react with ZrCo, forming ZrH_2 and ZrCo_2 directly. The pressure of the systems remains unchanged during the incubation process. Once disproportionation reaction goes through the incubation period, the hydrogen pressure decreases quickly. ZrCo absorbs H_2 and forms ZrH_2 and ZrCo_2 . ZrCo_2 cannot absorb hydrogen, and the decomposition temperature of ZrH_2 exceeds 973 K.^[21] This suggests that ZrH_2 and ZrCo_2 are thermally stable phases under experimental conditions, and the cyclic stability of $\text{ZrCo}_{1-x}\text{Cr}_x$ ($x = 0-0.1$) alloys deteriorates. Nucleation and nuclear growth process control the disproportionation rate of the ZrCo alloy.^[10,49] A fraction of ZrH_2 and ZrCo_2 , which formed during the incubation period may act as crystal nuclei of disproportionation reaction.^[49] ZrCo absorbs H_2 during which ZrH_2 and ZrCo_2 form along with the aforementioned products of the incubation period. The formation of ZrH_2 and ZrCo_2 generates more crystal nuclei of disproportionation reaction, which accelerates the disproportionation rate. The hydrogen pressure of the system decreases quickly in the first hour of reaction and then decreases slightly throughout the rest of the disproportionation process. The kinetics of the disproportionation reaction will be discussed in the next section in detail. As shown in Fig. 10, the maximum hydrogen pressure decreases gradually from 130.7 kPa to 106 kPa with an increase in the Cr content from 0 to 0.1. Hydrogen pressures of ZrCo-H and $\text{ZrCo}_{0.9}\text{Cr}_{0.1}$ -H systems decrease from 130.7 kPa and 106 kPa to 91.8 kPa and 75.4 kPa in 10 h. Table 5 shows the disproportionation behaviors of $\text{ZrCo}_{1-x}\text{Cr}_x$ ($x = 0-0.1$)-H systems. It is concluded that as the Cr content increases, the ability of anti-disproportionation

increases. In the study conducted by Zhang *et al.*,^[15] the disproportionation reaction of ZrCo finished within 400 min at 773 K. In this work, the hydrogen pressure decreases throughout the entire disproportionation process, which implies that the ZrCo sample has not been fully disproportionated. In Table 5, the initial pressures at 798 K are lower than the absorbed pressures for $\text{ZrCo}_{1-x}\text{Cr}_x$ ($x = 0.025-0.1$) alloys. This suggests that there are still residual hydrogen atoms in the matrix at 798 K; this part of the disproportionation reaction cannot be detected by the decrease in hydrogen pressure, and thus, the extent of disproportionation calculated from the decrease in hydrogen pressure are smaller. Once the furnace stopped heating after insulation at 798 K for 10 h, the hydrogen pressure gradually decreases for the remaining $\text{ZrCo}_{1-x}\text{Cr}_x$ ($x = 0-0.1$) alloys absorbed hydrogen to saturation again. The absorbed pressure and remaining pressure at room temperature are used to calculate the extents of disproportionation. The extents of disproportionation are calculated^[22] and listed in Table 5. It is evident in Table 5 that the ability of anti-disproportionation increases slightly with the increasing Cr concentration.

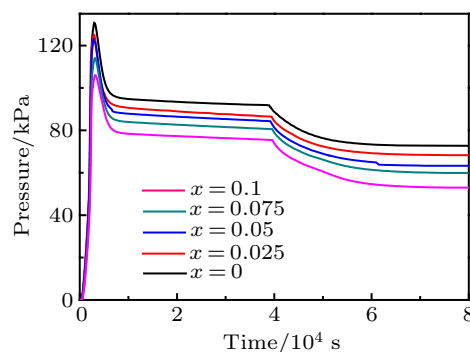


Fig. 10. Hydrogen pressure evolution of $\text{ZrCo}_{1-x}\text{Cr}_x$ ($x = 0-0.1$)-H systems at 798 K insulated for 10 h.

Table 5. Disproportionation behaviors of $\text{ZrCo}_{1-x}\text{Cr}_x$ ($x = 0-0.1$)-H systems at 798 K insulated for 10 h. Absorbed pressure is the change in hydrogen pressure of activation process at room temperature.

| Sample | Absorbed pressure/kPa | Initial pressure/kPa | Ending pressure/kPa | Remaining pressure/kPa | Extent of degradation/% |
|-------------|-----------------------|----------------------|---------------------|------------------------|-------------------------|
| $x = 0$ | 130.14 | 130.7 | 91.8 | 72.6 | 83.68 |
| $x = 0.025$ | 126.73 | 125.1 | 86.6 | 68.2 | 80.72 |
| $x = 0.05$ | 126.04 | 124 | 86.4 | 64.9 | 77.24 |
| $x = 0.075$ | 119.7 | 114 | 80.5 | 59.9 | 75.06 |
| $x = 0.1$ | 112.73 | 106 | 75.4 | 53 | 70.52 |

To confirm the extents of disproportionation decrease with the increase in the Cr content, the XRD spectra of $\text{ZrCo}_{1-x}\text{Cr}_x$ ($x = 0-0.1$) samples after the disproportionation process are shown in Fig. 11. The final products of the ZrCo-H system mainly consist of the ZrH_2 and ZrCo_2 phases, which indicate that the majority of $\text{ZrCo}_{1-x}\text{Cr}_x$ ($x = 0-0.1$) alloys are disproportionated. A fraction of the ZrCoH_3 phase is observed in all the alloys; meanwhile, the diffraction intensities of the ZrCoH_3 phase increase slightly with the increasing Cr

content. This suggests that the extents of disproportionation decrease slightly with the increase in the Cr content, which is in accordance with the calculated results in Table 5.

Considering hydrogen capacity, activation behaviors, hydrogen desorption plateau pressure, and disproportionation performance, the $\text{ZrCo}_{0.95}\text{Cr}_{0.05}$ alloy shows the optimum comprehensive performance. Systematically, disproportionation measurements for the ZrCo-H and $\text{ZrCo}_{0.95}\text{Cr}_{0.05}$ -H

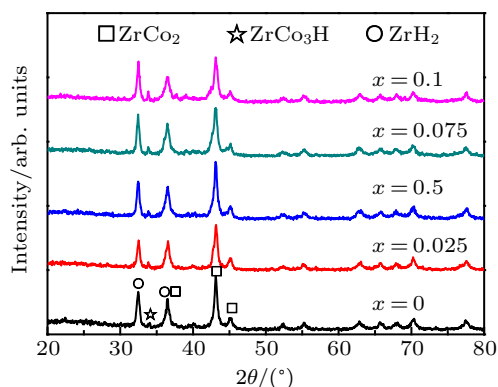


Fig. 11. XRD patterns of disproportionation products of $\text{ZrCo}_{1-x}\text{Cr}_x$ ($x=0-0.1$) alloys.

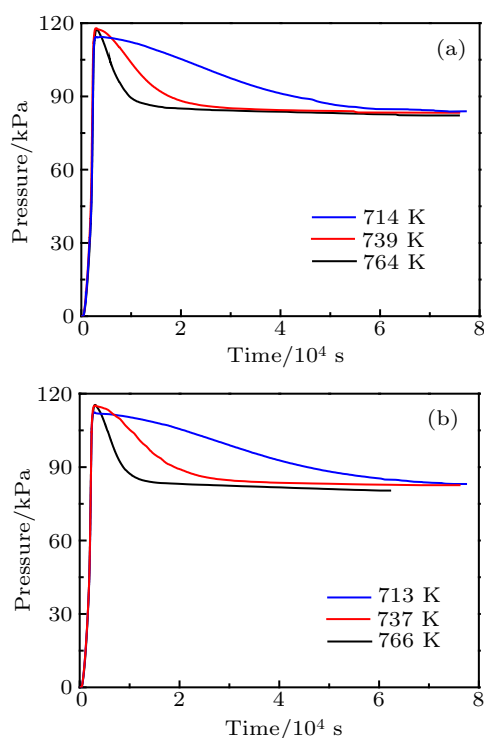


Fig. 12. The isothermal disproportionation curves of ZrCo (a) and $\text{ZrCo}_{0.95}\text{Cr}_{0.05}$ (b) samples.

systems were performed to further study the anti-disproportionation performance of Cr-alloyed alloys. The isothermal disproportionation curves of ZrCo and $\text{ZrCo}_{0.95}\text{Cr}_{0.05}$ alloys at different temperatures are shown in Fig. 12. Proper kinetic models have been adopted to fit the disproportionation curves. The first-order reaction (F1) model shows a good linear relationship with the disproportionation kinetics of ZrCo and $\text{ZrCo}_{0.95}\text{Cr}_{0.05}$.^[50,51] The disproportionation kinetics equation (Eq. (3))^[52] can be illustrated as

$$g(\alpha) = -\ln(1 - \alpha) = [k(T)t]^\eta, \quad (5)$$

where α is the reaction factor, $k(T)$ is the rate constant depended on the temperature, t is the reaction time, and η is the reaction order. Figure 13 depicts the linear plots of $\ln(-\ln(1 - \alpha))$ versus $\ln t$ for the disproportionation of ZrCo and $\text{ZrCo}_{0.95}\text{Cr}_{0.05}$ alloys at different temperatures. As shown

in Fig. 13, the fits (R^2) of the straight lines are > 0.996 , which indicates that the F1 model fits the reaction mechanism well.

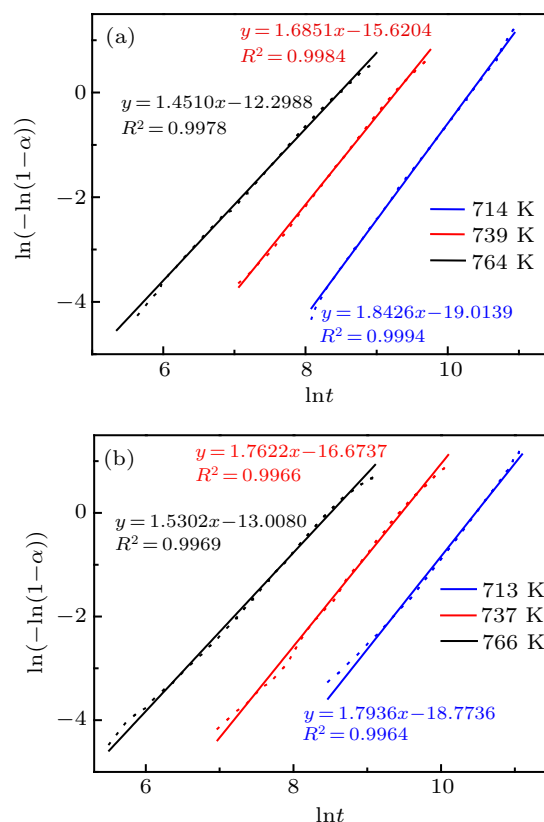


Fig. 13. Plots of $\ln(-\ln(1 - \alpha))$ versus $\ln t$ for the disproportionation of ZrCo (a) and $\text{ZrCo}_{0.95}\text{Cr}_{0.05}$ (b) alloys at different temperatures.

The apparent activation energy (E_{a2}) of the disproportionation reaction of ZrCo and $\text{ZrCo}_{0.95}\text{Cr}_{0.05}$ alloys can be calculated from the Arrhenius equation (Eq. (4))

$$k(T) = A \exp(-E_{a2}/RT), \quad (6)$$

where k is the rate constant obtained from Fig. 13. The linear plots of $\ln k$ versus $1000/T$ for the disproportionation reaction of ZrCo and $\text{ZrCo}_{0.95}\text{Cr}_{0.05}$ alloys are shown in Fig. 14. The E_{a2} for disproportionation of the ZrCo alloy which is calculated from the slope ($-E_{a2}/R$) of the fitted lines, is determined to be $167.46\text{-kJ}\cdot\text{mol}^{-1} \text{H}_2$ while that of $\text{ZrCo}_{0.95}\text{Cr}_{0.05}$ alloy increases to $168.28\text{-kJ}\cdot\text{mol}^{-1} \text{H}_2$. The fits (R^2) of the straight lines and the plots are > 0.992 , implying that the E_{a2} evaluated from the Arrhenius theory is reliable. The slight increase in E_{a2} agrees the slight decrease in the disproportionation kinetics. Here E_{a2} is considered as the energy barrier for the disproportionation; the change in E_{a2} is used to estimate the driving force of the disproportionation. E_{a2} increases after the alloying of Cr, suggesting that the substitution of Cr for Co increases the energy barrier for disproportionation, which improves the ability of the anti-disproportionation of Cr-alloyed alloys.

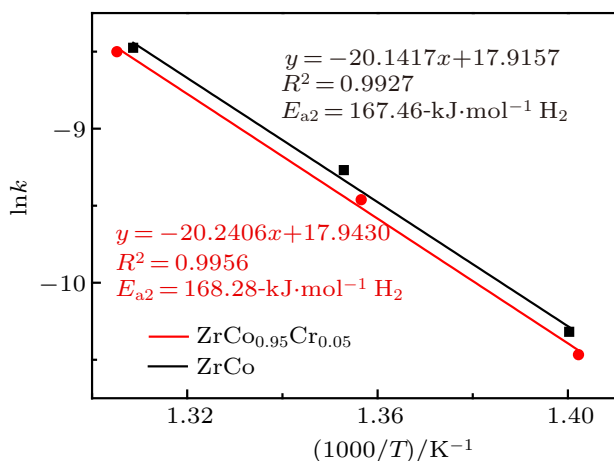


Fig. 14. Plots of $\ln k$ versus $1000/T$ for the disproportionation of ZrCo and $\text{ZrCo}_{0.95}\text{Cr}_{0.05}$ alloys.

4. Conclusions

The crystal structure, hydrogenation kinetics, thermodynamic characteristics, and disproportionation properties of $\text{ZrCo}_{1-x}\text{Cr}_x$ ($x = 0-0.1$) alloys were studied. The XRD spectra demonstrated that $\text{ZrCo}_{1-x}\text{Cr}_x$ ($x = 0-0.1$) alloys contained ZrCo and ZrCo_2 phases. The activation behaviors of Cr-substituted samples were significantly promoted. The activation time of ZrCo was 7715 s, while it decreased to 195 s for $\text{ZrCo}_{0.9}\text{Cr}_{0.1}$. According to the mechanism analysis, activation energy for hydrogenation decreased from $44.88\text{-kJ}\cdot\text{mol}^{-1}\text{H}_2$ for ZrCo to $40.34\text{-kJ}\cdot\text{mol}^{-1}\text{H}_2$ for $\text{ZrCo}_{0.95}\text{Cr}_{0.05}$. The thermodynamic results showed that the desorption plateau pressure decreased slightly with the increasing content of Cr. The extent of the disproportionation of ZrCo was 83.68% after being insulated at 798 K for 10 h; it decreased slightly to 70.52% for $\text{ZrCo}_{0.9}\text{Cr}_{0.1}$. The improvement of the anti-disproportionation performance can be attributed to the increase in activation energy of disproportionation from $167.46\text{-kJ}\cdot\text{mol}^{-1}\text{H}_2$ for ZrCo to $168.28\text{-kJ}\cdot\text{mol}^{-1}\text{H}_2$ for $\text{ZrCo}_{0.95}\text{Cr}_{0.05}$. The $\text{ZrCo}_{0.95}\text{Cr}_{0.05}$ alloy showed the optimum comprehensive performances in ITER.

References

- [1] Shmayda W T, Heics A G and Kherani N P 1990 *J. Less-common Metal* **162** 117
- [2] Li G, Zhou H and Gao T 2012 *J. Nucl. Mater.* **424** 220
- [3] Nagasaki T, Konishi S, Katsuta H and Naruse Y 1986 *J. Fusion Technol.* **9** 506
- [4] Konishi S, Nagasaki T, Yokokara N and Naruse Y 1989 *Fusion Eng. Des.* **10** 355
- [5] Devillers M, Sirch M, Bredendiek-Kaemper S and Penzhorn R D 1990 *J. Chem. Mater.* **2** 255
- [6] Maynard K J, Shmayda W T and Heics A G 1995 *J. Fusion Technol.* **28** 1391
- [7] Chattaraj D, Parida S C, Dash S and Majumder C 2012 *Int. J. Hydrogen Energy* **37** 18952
- [8] Peng L X, Jiang C L, Xu Q Y and Wu X C 2013 *Fusion Eng. Des.* **88** 299
- [9] Devillers M, Sirch M and Penzhorn R D 1992 *Chem. Mater.* **4** 631
- [10] Konishi S, Nagasaki T and Okuno K 1995 *J. Nucl. Mater.* **233** 294
- [11] Kou H Q, Luo W H, Tang T, Huang Z Y, Sang G, Wang H, Chen C A, Zhang G H, Bao J C and Xue Y 2018 *Int. J. Hydrogen Energy* **43** 16169
- [12] Kou H Q, He H, Luo W H, Tang T, Huang Z Y, Sang G, Zhang G H, Wang H, Shi Y and Chen C A 2018 *Int. J. Hydrogen Energy* **43** 322
- [13] Zlotea C, Sow M A, Gustav E, Couzinie J, Perriere L, Guillot I, Bourgon J, Moller K T, Jensen T R, Akiba E and Sahlberg M 2019 *J. Alloys Compd.* **775** 667
- [14] Ishikawa K and Yonehara K 2018 *J. Alloys Compd.* **749** 634
- [15] Zhang G H, Sang G, Xiong R J, Kou H Q, Liu K Z and Luo W H 2015 *Int. J. Hydrogen Energy* **40** 6582
- [16] Zhao Y M, Li R F, Tang R H, Li B Y, Yu R H, Liu W, Kou H Q and Meng J B 2014 *J. Energy Chem.* **23** 9
- [17] Jat R A, Parida S C, Agarwal R and Kulkarni S G 2013 *Int. J. Hydrogen Energy* **38** 1490
- [18] Weng C C, Xiao X Z, Huang X, Jiang F L, Yao Z D, Li S Q, Ge H W and Chen L X 2017 *Int. J. Hydrogen Energy* **42** 28498
- [19] Yao Z D, Xiao X Z, Liang Z, Kou H Q, Luo W H, Chen C A, Jiang L J and Chen L X 2019 *J. Alloys Compd.* **784** 1062
- [20] Jat R A, Singh R, Parida S C, Das A, Agarwal R, Mukerjee S and Ramakumar K L 2015 *Int. J. Hydrogen Energy* **40** 5135
- [21] Konishi S, Nagasaki T, Hayashi T and Okuno K 1995 *J. Nucl. Mater.* **223** 300
- [22] Jat R A, Singh R, Pati S, Sastry P U, Das A, Agarwal R and Padida S C 2017 *Int. J. Hydrogen Energy* **42** 8089
- [23] Luo L L, Ye X Q, Zhao C, Zhang G H, Kou H Q, Xiong R J, Sang G and Han T 2020 *Int. J. Hydrogen Energy* **45** 2989
- [24] Liang Z Q, Xiao X Z, Yao Z D, Kou H Q, Luo W H, Chen C A and Chen L X 2019 *Int. J. Hydrogen Energy* **44** 28242
- [25] Xu S F, Wang F, Tang W K, Wang Y B and Yu R H 2018 *Int. J. Hydrogen Energy* **43** 839
- [26] Zhang G H 2015 *Study on preparation and mechanism of ZrCo-based tritium storage alloys of anti-hydrogen induced disproportionation* (Anhui: University of Science and Technology of China) (in Chinese)
- [27] Zhang K, Wang F, Zeng X G, Zhang B J and Kou H Q 2020 *Int. J. Hydrogen Energy* **45** 9877
- [28] You Y W, Yu J Y, Yuan H, Xu Y C, Wu X B, Sun J J, Wang J H, Fang Q F and Liu C S 2020 *Int. J. Hydrogen Energy* **45** 14028
- [29] Wang L S, Ding J, Huang X, Song K, Liu B and Zeng X G 2018 *Int. J. Hydrogen Energy* **43** 13328
- [30] Wang F, Li R F, Ding C P, Tang W K, Wang Y B, Xu S M, Yu R H and Wang Z M 2017 *Int. J. Hydrogen Energy* **42** 11510
- [31] Yoo H, Ko J, Yun S, Chang M, Kang H, Kim W and Ju H 2012 *Int. J. Hydrogen Energy* **38** 6226
- [32] Wang F, Li R F, Ding C P, Wan J, Yu R H and Wang Z M 2016 *Int. J. Hydrogen Energy* **41** 17421
- [33] Kou H Q, He H, Luo W H, Tang T, Huang Z Y, Wang H, Bao J C, Xue Y, Pei S H and Liu W D 2019 *Fusion Eng. Des.* **138** 68
- [34] Kou H Q, Luo W H, Huang Z Y, Sang G, Hu C W, Chen C A, Zhang G H, Luo D L, Liu M and Zheng S T 2016 *Int. J. Hydrogen Energy* **41** 10811
- [35] Wang Q Q, Kong X G, Han H B, Sang G, Zhang G H and Gao T 2019 *Appl. Surf. Sci.* **483** 383
- [36] Lv L J 2016 *Study on improving properties of $\text{LaNi}_{4.25}\text{Al}_{0.75}$ and ZrCo alloys for absorption and storage of tritium in Thorium-based Molten Salt Reactor* (Shanghai: The University of Chinese Academy of Sciences) (in Chinese)
- [37] Yao Z D, Xiao X X, Chen L X and Liang Z Q 2018 *Chinese Patent* CN108330323A (in Chinese)
- [38] 1990 *Plus updates Binary alloy phase diagrams*, 2nd edn. (ASM International) The Materials Information Society
- [39] 1992 *Alloy Phase Diagrams*, Volume 3, *ASM Handbook*, The Materials Information Company
- [40] Jacob I and Polak M 1981 *J. Mater. Res. Bull.* **16** 1311
- [41] Schlapbach L 1982 *J. Alloys Compd.* **89** 37
- [42] Edalati K, Matsuo M, Emami H, Itano S, Alhamidi A, Staykov A T, Smith D J, Orimo S, Akiba E and Horita Z 2016 *Scr. Mater.* **124** 108
- [43] Zander D, Talgutmacher E, Jastrow L, Koster U and Eliezzer D 2003 *J. Alloys Compd.* **356** 654

- [44] Jat R A, Parida S C, Nuwad J, Agarwal R and Kulkarni S G 2013 *J. Therm. Anal. Calorim.* **112** 37
- [45] Li Y T, Zhang L X, Zhang Q G, Fang F, Sun D L, Li K Z, Wang H, Ouyang L Z and Zhu M 2014 *J. Phys. Chem. C* **118** 23635
- [46] Liu T, Cao Y R, Qin C G, Chou W S and Li X G 2014 *J. Power Sources* **246** 277
- [47] Qi Y, Ju X, Wan C B, Qiu J, Xin Y, Wang S M, Liu X P and Jiang L J 2010 *Int. J. Hydrogen Energy* **35** 2931
- [48] Shim M, Chung H, Paek S, Lee M, Kim K, Yim S, Ahn D, Kim C and Yoshida H 2006 *J. Korean Phys. Soc.* **49** S369
- [49] Hara M, Okabe T, Mori K and Watanabe K 2000 *J. Fusion Eng. Des.* **49** 831
- [50] Zhang Y, Tian Q F, Zhang J, Liu S S and Sun L X 2009 *J. Phys. Chem. C* **113** 18424
- [51] Liu Y F, Zhong K, Luo K, Gao X M, Pan H G, Wang Q D 2009 *J. Am. Chem. Soc.* **131** 1862
- [52] Shao J 2015 *Study on the modification and corresponding mechanisms of lithium borohydride-based materials for hydrogen storage* (Hangzhou: Zhejiang University) (in Chinese)